Cross-scale energy transfer of chaotic oscillator chain in stiffness-dominated range

Jian-en Chen
Tianjin University of Technology
Min Sun (sunmin0537@163.com)
Tianjin Chengjian University https://orcid.org/0000-0002-2632-1393
Wei Zhang
Beijing University of Technology
Shuang-bao Li
Civil Aviation University of China
Rui-qin Wu
Tianjin University of Technology

Research Article

Keywords: Energy transfer, cross-scale, chaotic response, stiffness-dominated range

Posted Date: April 5th, 2022

DOI: https://doi.org/10.21203/rs.3.rs-1508740/v1

Abstract

The investigations on the dynamics of hierarchical oscillator chains provide basic theories for the fields of acoustic metamaterial and passive guidance of energy flow. In the present study, the characteristics of stiffness-dominated energy transfer of a reduced cross-scale oscillator chain that generates chaotic vibrations are studied. The semi-analytical solutions are obtained by the complexification-averaging method and the least-square method for thoroughly searching the branches of responses. Then the energy transfer patterns of the oscillator chain are analyzed based on Runge-Kutta method. Moreover, chaotic responses are determined using the displacements and Lyapunov exponents of the system. The average energy and normalized energy flux are defined to evaluate the energy distribution in each oscillator and the energy transfer between oscillators, respectively. The semi-analytical results show that the oscillator chain produces complex unstable branches of response around the resonance frequency of the linear oscillator. It is found that the detached higher branches of response of the chain are similar to that of a system consisting of one linear oscillator and one cubic oscillator. When chaotic responses occur, the energy transfer patterns that reflected by average energy and normalized energy flux are similar in the same branch of response for different excitation frequencies. However, energy transfer patterns in different branches of response are quite different even at the same excitation frequency, and the higher branch generates the lower energy transfer. Furthermore, analyses of the input energy and the scale between cubic oscillators demonstrate that variations of the two parameters slightly affect the normalized energy flux.

1. Introduction

Energy transfer such as energy transfer between vortices in turbulent flows, energy transfer between molecules through heat conduction, and solar energy transfer to plants through photosynthesis occurs widely in nature. With the development and maturity of the nonlinear theory, nonlinear elements have been added into various linear systems to improve their performances [1, 2], and construct the so-called artificial nonlinear systems. Accordingly, the construction of various nonlinear paths has become a research hotspot to achieve the expected energy transfer in mechanical and acoustic systems [3, 4].

Usually, turbulent flows are considered as a typical example of the cross-scale energy transfer between vortices of different scales where large and unstable vortices break up into several smaller ones, thereby irreversibly transferring energy from larger scales to small scales. Based on the idea of decreasing scale binomial tree network, an equivalent decreasing scale oscillator chain has been used to simulate the energy transfer in turbulent flows. Through parameter adjustment, energy transfer between oscillators in the chain is in accordance with the well-known Kolmogorov law [5]. This study is helpful to find some general rules of energy transfer between oscillators and has the potential to provide a new angle for the study of fluid turbulence. The models comprise linear and weakly nonlinear oscillator chains respectively, were both studied [6, 7]. To explore the similarities of energy transfer between chaotic mechanical system and fluid turbulence, a model consisting of a linear oscillator and purely cubic oscillators was proposed,

and the irreversible energy transfer from stiffness-dominated larger scales to damping-dominated smaller scales was analyzed [8].

Reviewing the literature indicates that predictable designs for nonlinear targeted energy transfer motivated by fluid turbulence have been investigated for more than two decades [9]. Nonlinear energy sink (NES) is a representative application of the principle of targeted energy transfer, where the energy transfer path constructed by purely cubic nonlinearity, and has been widely studied so far [10–12]. To improve the efficiency of energy transfer, several components have been considered to modify the standard NES, thereby forming several novel vibration absorption devices such as lever-type [13], limited-type [14, 15], encapsulated-type [16], collision enhanced-type [17], inertial-type [18], and stiffness descending-type [19]. Recently, studies about NESs have merged with energy harvesting, which is another hot research topic that concentrates on the energy transfer between mechanical and electrical sources of energy [20, 21]. In view of the bright prospects of NESs, investigations about the energy transfer between vibratory systems and NESs are expected to be continued for a long time.

In the past few years, the nonreciprocity of energy transfer has attracted special attention, which has become a challenging issue in the fields of acoustic and mechanical metamaterials and can be considered as a modified irreversible energy transfer. The nonreciprocity of energy transfer was analyzed for a reduced two-degree-of-freedom model with purely nonlinear and asymmetric oscillators, demonstrating that the transient resonance energy capture is an important phenomenon that should be considered to realize nonreciprocity [22]. Accordingly, the linear and purely nonlinear oscillators were utilized to construct decreasing-scale oscillator chains with different structures [23] and periodic oscillator chains with several identical cells to achieve global nonreciprocity [24]. Subsequently, the direction control of energy transfer in an oscillator network was achieved by using purely nonlinear components, which expands the application of non-reciprocity [25].

Currently, most investigations in this area are mainly concentrated on the vibration absorption of cubic oscillators. In this regard, NESs with two and multiple degrees-of-freedom, which can be seemed as reduced oscillator chains, have been used to suppress vibrations of impulsively and harmonically excited linear primary systems [26–29], aeroelastic instability of a rigid wing with structural nonlinearities [30], and responses of a six-story structure subjected to a shock-type loading [31]. Considering the limitations of the vibration absorber structure, equal-weight cubic oscillators are usually used (at least the weight of the oscillators are close). Accordingly, the energy transfer between such cubic oscillators is an equi-scale phenomenon.

In the present study, nonlinear energy transfer in a cross-scale chain with a linear oscillator and three cubic oscillators is analyzed when the stiffness-dominated chaotic responses are excited. The energy transfer patterns in the oscillator chain are explored using the Runge-Kutta, complexification-averaging, and least-square methods. It is intended to study the characteristics of energy transfer of the chain with different steady-state responses by analyzing the average energy and normalized energy flux. The main

objective of this study is to find and investigate differences and similarities of different intense energy transfers produced in the cross-scale oscillator chain.

2. Reduced Model Of The Stiffness-dominated Range

Figure 1 shows a nonlinear hierarchical oscillator chain consisting of a harmonically excited linear oscillator and *N* purely cubic nonlinear oscillators. *M*, *K* and μ denote mass, linear stiffness, and viscous damping coefficients of the primary linear oscillator, respectively. Moreover, m_n, k_n and λ_n $(n = 1, \ldots, N)$ denote the mass, cubic stiffness, and viscous damping coefficients of the cubic oscillators, respectively. x_{n+1}, $n = 0, 1, \ldots, N$ reflects the displacements of $N + 1$ oscillators of the system. The linear oscillator is excited by a harmonic excitation represented by $f\cos(\Omega t)$, where f and Ω are the excitation amplitude and frequency, respectively.

The governing equations of the oscillator chain can be expressed as follows [8]:

$$M\ddot{x}_1 + \mu\dot{x}_1 + Kx_1 + \lambda_1(\dot{x}_1 - \dot{x}_2) + k_1(x_1 - x_2)^3 = f\cos(\Omega t)$$

1a

$$m_n\ddot{x}_{n+1} + \lambda_n(\dot{x}_{n+1} - \dot{x}_n) + k_n(x_{n+1} - x_n)^3$$

$$+\lambda_{n+1}(\dot{x}_{n+1} - \dot{x}_{n+2}) + k_{n+1}(x_{n+1} - x_{n+2})^3 = 0, n = 1, 2 \cdots N-1 \text{ (1b)}$$

$$m_N\ddot{x}_{N+1} + \lambda_N(\dot{x}_{N+1} - \dot{x}_N) + k_N(x_{N+1} - x_N)^3 = 0$$

1c

Introducing the following normalized variables and parameters

$$\varepsilon_n = \frac{m_n}{M}, \tilde{t} = \sqrt{\frac{K}{M}}t, \tilde{\mu} = \frac{\mu}{\sqrt{KM}}, \tilde{\lambda} = \frac{\lambda}{\sqrt{KM}}, \tilde{k}_n = \frac{k_n}{K}, \tilde{f} = \frac{f}{K}, \tilde{\Omega} = \sqrt{\frac{M}{K}}\Omega.$$

Equations (1a)-(1c) can be rewritten in the following non-dimensional form:

$$\ddot{x}_1 + \tilde{\mu}\dot{x}_1 + x_1 + \tilde{\lambda}_1(\dot{x}_1 - \dot{x}_2) + \tilde{k}_1(x_1 - x_2)^3 = \tilde{f}\cos(\tilde{\Omega}\tilde{t})$$

2a

$$\varepsilon_n\ddot{x}_{n+1} + \tilde{\lambda}_n(\dot{x}_{n+1} - \dot{x}_n) + \tilde{k}_n(x_{n+1} - x_n)^3$$

$$+\tilde{\lambda}_{n+1}(\dot{x}_{n+1} - \dot{x}_{n+2}) + \tilde{k}_{n+1}(x_{n+1} - x_{n+2})^3 = 0, n = 1, 2 \cdots N-1 \text{ (2b)}$$

$$\varepsilon_N\ddot{x}_{N+1} + \tilde{\lambda}_N(\dot{x}_{N+1} - \dot{x}_N) + \tilde{k}_N(x_{N+1} - x_N)^3 = 0$$

2c

For the convenience of writing, the tildes superscript will be dropped in the subsequent analysis. The hierarchy of scales can be achieved by decreasing the system parameters from the left oscillator to the right one according to the following scaling laws:

$$\frac{\varepsilon_{n-1}}{\varepsilon_n} = 8, \frac{k_{n-1}}{k_n} = 30, \frac{\lambda_{n-1}}{\lambda_n} = 2, n = 2,\ 3,\ \ldots, N$$

It is worth noting that the system parameters of the linear oscillator are μ=0.01, ε_1=0.05, $k_1 = 0.5$, and λ_1=0.001.

Figure 2 shows the average energy of each oscillator in different chains. The average steady-state energy in the linear (E_{L_O}) and nonlinear oscillators (E_n) can be expressed as follows:

$$E_{L_O} = \frac{1}{T}\int_{t_0}^{t_0+T}(\frac{1}{2}(\dot{x}_1^2 + x_1^2) + \frac{1}{8}k_1(x_1 - x_2)^4)\,dt$$

3a

,

$$E_n = \frac{1}{T}\int_{t_0}^{t_0+T}(\frac{1}{2}\varepsilon_n\dot{x}_{n+1}^2 + \frac{1}{8}k_n(x_n - x_{n+1})^4 + \frac{1}{8}k_{n+1}(x_{n+1} - x_{n+2})^4)\,dt$$

,

$$n = 1,\ 2, \ldots,\ N$$

3b

,

where {t_0}=2000 and T=1000, indicating that a long enough initial time is removed to reach steady-state vibrations.

It is shown that the energy in the stiffness-dominated (large-scale) range is much larger than that in the damping-dominated (small-scale) range. The *x* and *y* axes both uses logarithmic coordinates in Fig. 2, and the mass scales are defined as 1/{\varepsilon _n}, n=1,\;2...N, and the mass scale corresponding to the linear oscillator is normalized to unity. The line of Kolmogorov power law can be used as a reference to distinguish the occurrence of chaotic motions. Moreover, the energies in chains with three, six, and nine cubic oscillators are compared. It is found that when the input energy is at a low level (excitation amplitude is small), it hardly transfers to small scales. However, when the input energy reaches a certain level, the energy level in cubic oscillators of different chains enhances dramatically. It is observed that the three lines in each sub-figures coincide with each other and as the input energy increases, the differences between the three lines increase continuously. Figures 2(b)-2(d) reveal that the blue and red lines all have two regions, the lines in one region is almost parallel with -axis and the lines in the other one decreases according to a power law.

Figure 3 shows the distribution of the coupling force {F_n} versus the relative displacements and velocities for oscillators in a chain with six cubic oscillators. In this way, the influence of cubic stiffness nonlinearities and the linear viscous dissipative forces on the energy transfer process can be investigated. The coupling force can be calculated using the following expression:

{F_n}={k_n}({x_n} - {x_{n+1}})^3}+{\lambda _n}({\dot {x}_n} - {\dot {x}_{n+1}}), n=1,\;2\; \cdots \;N. (4)

Figure 3 shows that the dynamics of the first three cubic oscillators are dominated by the stiffness nonlinearity (i.e., the relation between coupling force and relative displacement is cubic), while the motions of the last three cubic oscillators are mainly affected by the linear damping (i. e., the relation between coupling force and relative velocity is linear). Based on Figs. 2 and 3, a reduced mechanical model of Fig. 1 (i.e., N=3) can be established to study the energy transfer and dynamics in the stiffness-dominated range of the cross-scale oscillator chain. Another advantage of using the reduced model is that the analytical procedure can be significantly simplified. When N=3, Eq. (2) can be rewritten in the form below:

{\ddot {x}_1}+\mu {\dot {x}_1}+{x_1}+{\lambda _1}({\dot {x}_1} - {\dot {x}_2})+{k_1}({x_1} - {x_2})^3}=f\cos (\Omega t), (5a)

{\varepsilon _1}{\ddot {x}_2}+{\lambda _1}({\dot {x}_2} - {\dot {x}_1})+{k_1}({x_2} - {x_1})^3}{\text{+}} {\lambda _2}({\dot {x}_2} - {\dot {x}_3})+{k_2}({x_2} - {x_3})^3}=0
5b
,

{\varepsilon _2}{\ddot {x}_3}+{\lambda _2}({\dot {x}_3} - {\dot {x}_2})+{k_2}({x_3} - {x_2})^3}{\text{+}} {\lambda _3}({\dot {x}_3} - {\dot {x}_4})+{k_3}({x_3} - {x_4})^3}=0
5c
,

{\varepsilon _3}{\ddot {x}_4}+{\lambda _3}({\dot {x}_4} - {\dot {x}_3})+{k_3}({x_4} - {x_3})^3}=0
5d

3. Energy Transfer In Oscillator Chain

In this section, the complexification-averaging method is used to obtain the first-order equation and analyze the distribution of the system response in frequency bands. To this end, the following transformations are introduced:

Lets{u_1}={x_1}, {u_k}={x_{k - 1}} - {x_k}, k=2\,\;3\,\;4, and introduce the following transformations:

{\dot {u}_k}+i\Omega {u_k}={\partial _k}{e^{i\Omega t}}, k=1\,\; \cdots \,\;4 (6)

Subsequently, these expressions can be obtained:

{u_k}=\frac{{{\partial _k}{e^{i\Omega t}} - {{\bar {\partial }}_k}{e^{ - i\Omega t}}}}{{2i\Omega }}, {\dot {u}_k}=\frac{{{\partial _k}{e^{i\Omega t}}+{{\bar {\partial }}_k}{e^{ - i\Omega t}}}}{2},

{\ddot {u}_k}=\frac{{{{\dot {\partial }}_k}{e^{i\Omega t}}+i\Omega {e^{i\Omega t}}{\partial _k}+{{\dot {\bar {\partial }}}_k}{e^{ - i\Omega t}} - i\Omega {e^{i\Omega t}}{{\bar {\partial }}_k}}}{2}
7
Substituting expression (7) into Eq. (5) and retaining the slow flow parts results in the following expressions:

{\dot {\partial }_1}+i\Omega {\partial _1}+\mu {\partial _1}+\frac{{{\partial _1}}}{{i\Omega }}+{\lambda _1}{\partial _2} - \frac{{3{k_1}{\partial _2}^{2}{{\bar {\partial }}_2}}}{{4{i^3}{\Omega ^3}}}=f
8a
,

{\varepsilon _1}\left({{{\dot {\partial }}_1}+i\Omega {\partial _1} - {{\dot {\partial }}_2} - i\Omega {\partial _2}} \right) - {\lambda _1}{\partial _2}+\frac{{3{k_1}{\partial _2}^{2}{{\bar {\partial }}_2}}}{{4{i^3}{\Omega ^3}}}+{\lambda _2}{\partial _3} - \frac{{3{k_2}{\partial _3}^{2}{{\bar {\partial }}_3}}}{{4{i^3}{\Omega ^3}}}=0
8b
,

{\varepsilon _2}\left({{{\dot {\partial }}_1}+i\Omega {\partial _1} - {{\dot {\partial }}_2} - i\Omega {\partial _2} - {{\dot {\partial }}_3} - i\Omega {\partial _3}} \right) - {\lambda _2}{\partial _3}+\frac{{3{k_2}{\partial _3}^{2}{{\bar {\partial }}_3}}}{{4{i^3}{\Omega ^3}}}+{\lambda _3}{\partial _4} - \frac{{3{k_3}{\partial _4}^{2}{{\bar {\partial }}_4}}}{{4{i^3}{\Omega ^3}}}=0
8c
,

{\varepsilon _3}\left({{{\dot {\partial }}_1}+i\Omega {\partial _1} - {{\dot {\partial }}_2} - i\Omega {\partial _2} - {{\dot {\partial }}_3} - i\Omega {\partial _3} - {{\dot {\partial }}_4} - i\Omega {\partial _4}} \right) - {\lambda _3}{\partial _4}+\frac{{3{k_3}{\partial _4}^{2}{{\bar {\partial }}_4}}}{{4{i^3}{\Omega ^3}}}=0
8d
Introducing {\partial _k}={a_k}+i{b_k}, k=1\,,\; \cdots \,,\;4 into Eq. (8) yields:

{\dot {a}_1}+i{\dot {b}_1}+i\Omega \left({{a_1}+i{b_1}} \right)+\mu \left({{a_1}+i{b_1}} \right)+\frac{{{a_1}+i{b_1}}}{{i\Omega }}+{\lambda _1}\left({{a_2}+i{b_2}} \right)

- \frac{{3i{k_1}\left({{a_2}^{2}+{b_2}^{2}} \right)\left({{a_2}+i{b_2}} \right)}}{{4{\Omega ^3}}}=f
9a
,

{\varepsilon _1}\left[{{{\dot {a}}_1}+i{{\dot {b}}_1}+i\Omega \left({{a_1}+i{b_1}} \right) - {{\dot {a}}_2} - i{{\dot {b}}_2} - i\Omega \left({{a_2}+i{b_2}} \right)} \right] - {\lambda _1}\left({{a_2}+i{b_2}} \right)+\frac{{3i{k_1}\left({{a_2}^{2}+{b_2}^{2}} \right)\left({{a_2}+i{b_2}} \right)}}{{4{\Omega ^3}}} +

{\lambda _2}\left({{a_3}+i{b_3}} \right) - \frac{{3i{k_2}\left({{a_3}^{2}+{b_3}^{2}} \right)\left({{a_3}+i{b_3}} \right)}}{{4{\Omega ^3}}}=0, (9b)

{\varepsilon _2}\left[{{{\dot {a}}_1}+i{{\dot {b}}_1}+i\Omega \left({{a_1}+i{b_1}} \right) - {{\dot {a}}_2} - i{{\dot {b}}_2} - i\Omega \left({{a_2}+i{b_2}} \right) - {{\dot {a}}_3} - i{{\dot {b}}_3} - i\Omega \left({{a_3}+i{b_3}} \right)} \right]

- {\lambda _2}\left({{a_3}+i{b_3}} \right)+\frac{{3i{k_2}\left({{a_3}^{2}+{b_3}^{2}} \right)\left({{a_3}+i{b_3}} \right)}}{{4{\Omega ^3}}}+{\lambda _3}\left({{a_4}+i{b_4}} \right) - \frac{{3i{k_3}\left({{a_4}^{2}+{b_4}^{2}} \right)\left({{a_4}+i{b_4}} \right)}}{{4{\Omega ^3}}}
9c
,

{\varepsilon _3}\left[{{{\dot {a}}_1}+i{{\dot {b}}_1}+i\Omega \left({{a_1}+i{b_1}} \right) - {{\dot {a}}_2} - i{{\dot {b}}_2} - i\Omega \left({{a_2}+i{b_2}} \right) - {{\dot {a}}_3} - i{{\dot {b}}_3} - i\Omega \left({{a_3}+i{b_3}} \right)} \right.

\left. { - {{\dot {a}}_4} - i{{\dot {b}}_4} - i\Omega \left({{a_4}+i{b_4}} \right)} \right] - {\lambda _3}\left({{a_4}+i{b_4}} \right)+\frac{{3i{k_3}\left({{a_4}^{2}+{b_4}^{2}} \right)\left({{a_4}+i{b_4}} \right)}}{{4{\Omega ^3}}}=0
9d
Then the real and imaginary parts of Eq. (9) can be separated in the form below:

{\dot {a}_1} - \Omega {b_1}+\mu {a_1}+\frac{{{b_1}}}{\Omega }+{\lambda _1}{a_2}+\frac{{3{k_1}\left({{a_2}^{2}+{b_2}^{2}} \right){b_2}}}{{4{\Omega ^3}}}=f
10a
,

{\dot {b}_1}+\Omega {a_1}+\mu {b_1} - \frac{{{a_1}}}{\Omega }+{\lambda _1}{b_2} - \frac{{3{k_1}\left({{a_2}^{2}+{b_2}^{2}} \right){a_2}}}{{4{\Omega ^3}}}=0
10b
,

{\varepsilon _1}\left[{{{\dot {a}}_1} - \Omega {b_1} - {{\dot {a}}_2}+\Omega {b_2}} \right] - {\lambda _1}{a_2} - \frac{{3{k_1}\left({{a_2}^{2}+{b_2}^{2}} \right){b_2}}}{{4{\Omega ^3}}}+{\lambda _2}{a_3}+\frac{{3{k_2}\left({{a_3}^{2}+{b_3}^{2}} \right){b_3}}}{{4{\Omega ^3}}}=0
10c
,

{\varepsilon _1}\left[{{{\dot {b}}_1}+\Omega {a_1} - {{\dot {b}}_2} - \Omega {a_2}} \right] - {\lambda _1}{b_2}+\frac{{3{k_1}\left({{a_2}^{2}+{b_2}^{2}} \right){a_2}}}{{4{\Omega ^3}}}+{\lambda _2}{b_3} - \frac{{3{k_2}\left({{a_3}^{2}+{b_3}^{2}} \right){a_3}}}{{4{\Omega ^3}}}=0
10d

,

{\varepsilon _2}\left[{{{\dot {a}}_1} - \Omega {b_1} - {{\dot {a}}_2}+\Omega {b_2} - {{\dot {a}}_3}+\Omega {b_3}} \right] - {\lambda _2}{a_3} - \frac{{3{k_2}\left({{a_3}^{2}+{b_3}^{2}} \right){b_3}}}{{4{\Omega ^3}}}

+{\lambda _3}{a_4}+\frac{{3{k_3}\left({{a_4}^{2}+{b_4}^{2}} \right){b_4}}}{{4{\Omega ^3}}}=0
10e

,

{\varepsilon _2}\left[{{{\dot {b}}_1}+\Omega {a_1} - {{\dot {b}}_2} - \Omega {a_2} - {{\dot {b}}_3} - \Omega {a_3}} \right] - {\lambda _2}{b_3}+\frac{{3{k_2}\left({{a_3}^{2}+{b_3}^{2}} \right){a_3}}}{{4{\Omega ^3}}}

+{\lambda _3}{b_4} - \frac{{3{k_3}\left({{a_4}^{2}+{b_4}^{2}} \right){a_4}}}{{4{\Omega ^3}}}=0
10f

,

{\varepsilon _3}\left[{{{\dot {a}}_1} - \Omega {b_1} - {{\dot {a}}_2}+\Omega {b_2} - {{\dot {a}}_3}+\Omega {b_3} - {{\dot {a}}_4}+\Omega {b_4}} \right] - {\lambda _3}{a_4} - \frac{{3{k_3}\left({{a_4}^{2}+{b_4}^{2}} \right){b_4}}}{{4{\Omega ^3}}}=0
10g

,

{\varepsilon _3}\left[{{{\dot {b}}_1}+\Omega {a_1} - {{\dot {b}}_2} - \Omega {a_2} - {{\dot {b}}_3} - \Omega {a_3} - {{\dot {b}}_4} - \Omega {a_4}} \right] - {\lambda _3}{b_4}+\frac{{3{k_3}\left({{a_4}^{2}+{b_4}^{2}} \right){a_4}}}{{4{\Omega ^3}}}=0
10h

.

Then these equations can be derived based on Eq. (10):

{\dot {a}_1}=\Omega {b_1} - \mu {a_1} - \frac{{{b_1}}}{\Omega } - {\lambda _1}{a_2} - \frac{{3{k_1}\left({{a_2}^{2}+{b_2}^{2}} \right){b_2}}}{{4{\Omega ^3}}}+f
11a

,

{\dot {b}_1}= - \Omega {a_1} - \mu {b_1}{\text{+}}\frac{{{a_1}}}{\Omega } - {\lambda _1}{b_2}+\frac{{3{k_1}\left({{a_2}^{2}+{b_2}^{2}} \right){a_2}}}{{4{\Omega ^3}}}
11b

,

{\dot {a}_2}= - \mu {a_1} - \frac{{{b_1}}}{\Omega } - {\lambda _1}{a_2} - \frac{{3{k_1}\left({{a_2}^{2}+{b_2}^{2}} \right){b_2}}}{{4{\Omega ^3}}}+f+\Omega {b_2} - \frac{{{\lambda _1}{a_2}}}{{{\varepsilon _1}}} - \frac{{3{k_1}\left({{a_2}^{2}+{b_2}^{2}} \right){b_2}}}{{4{\Omega ^3}{\varepsilon _1}}}

+\frac{{{\lambda _2}{a_3}}}{{{\varepsilon _1}}}+\frac{{3{k_2}\left({{a_3}^{2}+{b_3}^{2}} \right){b_3}}}{{4{\Omega ^3}{\varepsilon _1}}}

11c

,

{\dot {b}_2}= - \mu {b_1}+\frac{{{a_1}}}{\Omega } - {\lambda _1}{b_2}+\frac{{3{k_1}\left({{a_2}^{2}+{b_2}^{2}} \right){a_2}}}{{4{\Omega ^3}}} - \Omega {a_2} - \frac{{{\lambda _1}{b_2}}}{{{\varepsilon _1}}}+\frac{{3{k_1}\left({{a_2}^{2}+{b_2}^{2}} \right){a_2}}}{{4{\Omega ^3}{\varepsilon _1}}}

+\frac{{{\lambda _2}{b_3}}}{{{\varepsilon _1}}} - \frac{{3{k_2}\left({{a_3}^{2}+{b_3}^{2}} \right){a_3}}}{{4{\Omega ^3}{\varepsilon _1}}}

11d

,

{\dot {a}_3}=\frac{{{\lambda _1}{a_2}}}{{{\varepsilon _1}}}+\frac{{3{k_1}\left({{a_2}^{2}+{b_2}^{2}} \right){b_2}}}{{4{\Omega ^3}{\varepsilon _1}}} - \frac{{{\lambda _2}{a_3}}}{{{\varepsilon _1}}} - \frac{{3{k_2}\left({{a_3}^{2}+{b_3}^{2}} \right){b_3}}}{{4{\Omega ^3}{\varepsilon _1}}}+\Omega {b_3} - \frac{{{\lambda _2}{a_3}}}{{{\varepsilon _2}}}+\frac{{{\lambda _3}{a_4}}}{{{\varepsilon _2}}}

- \frac{{3{k_2}\left({{a_3}^{2}+{b_3}^{2}} \right){b_3}}}{{4{\Omega ^3}{\varepsilon _2}}}+\frac{{3{k_3}\left({{a_4}^{2}+{b_4}^{2}} \right){b_4}}}{{4{\Omega ^3}{\varepsilon _2}}}

11e

,

{\dot {b}_3}=\frac{{{\lambda _1}{b_2}}}{{{\varepsilon _1}}} - \frac{{3{k_1}\left({{a_2}^{2}+{b_2}^{2}} \right){a_2}}}{{4{\Omega ^3}{\varepsilon _1}}} - \frac{{{\lambda _2}{b_3}}}{{{\varepsilon _1}}}+\frac{{3{k_2}\left({{a_3}^{2}+{b_3}^{2}} \right){a_3}}}{{4{\Omega ^3}{\varepsilon _1}}} - \Omega {a_3} - \frac{{{\lambda _2}{b_3}}}{{{\varepsilon _2}}}+\frac{{{\lambda _3}{b_4}}}{{{\varepsilon _2}}}

+\frac{{3{k_2}\left({{a_3}^{2}+{b_3}^{2}} \right){a_3}}}{{4{\Omega ^3}{\varepsilon _2}}} - \frac{{3{k_3}\left({{a_4}^{2}+{b_4}^{2}} \right){a_4}}}{{4{\Omega ^3}{\varepsilon _2}}}

11f

,

{\dot {a}_4}=\frac{{{\lambda _2}{a_3}}}{{{\varepsilon _2}}} - \frac{{{\lambda _3}{a_4}}}{{{\varepsilon _2}}}+\frac{{3{k_2}\left({{a_3}^{2}+{b_3}^{2}} \right){b_3}}}{{4{\Omega ^3}{\varepsilon _2}}} - \frac{{3{k_3}\left({{a_4}^{2}+{b_4}^{2}} \right){b_4}}}{{4{\Omega ^3}{\varepsilon _2}}}+\Omega {b_4}

- \frac{{{\lambda _3}{a_4}}}{{{\varepsilon _3}}} - \frac{{3{k_3}\left({{a_4}^{2}+{b_4}^{2}} \right){b_4}}}{{4{\Omega ^3}{\varepsilon _3}}}

11g

,

{\dot {b}_4}=\frac{{{\lambda _2}{b_3}}}{{{\varepsilon _2}}} - \frac{{{\lambda _3}{b_4}}}{{{\varepsilon _2}}} - \frac{{3{k_2}\left({{a_3}^{2}+{b_3}^{2}} \right){a_3}}}{{4{\Omega ^3}{\varepsilon _2}}}+\frac{{3{k_3}\left({{a_4}^{2}+{b_4}^{2}} \right){a_4}}}{{4{\Omega ^3}{\varepsilon _2}}} - \Omega {a_4}

- \frac{{{\lambda _3}{b_4}}}{{{\varepsilon _3}}}+\frac{{3{k_3}\left({{a_4}^{2}+{b_4}^{2}} \right){a_4}}}{{4{\Omega ^3}{\varepsilon _3}}}
11h
.

In order to obtain the steady-state response of the system, we set {\dot {a}_n}=0, {\dot {b}_n}=0, n=1,\;2,\;3,\;4. Furthermore, the amplitude of an oscillator can be calculated by A=\frac{{\sqrt {a_{n}^{2}+b_{n}^{2}} }}{\Omega }.

To verify the accuracy of the calculation, the results of the complexification-averaging method are compared with that of the Runge-Kutta method. To this end, the steady-state response equations of the system (11) are solved by using a code based on least square method and Eq. (5) is solved directly by using Runge-Kutta method, respectively. It should be indicated that these equations are both solved in the Matlab software environment. In Fig. 4, the black and red points denote the stable and unstable solutions from complexification-averaging method and least square method, and blue circles denotes the solutions from Runge-Kutta method. Figure 4 reveals that the results in the stable region of Fig. 4(a) and in the lower stable branch of Fig. 4(b) obtained by the two methods are consistent. It is worth noting that the values of the blue circles are the maximal values of the displacement in the selected time window. Therefore, there are some deviations in unstable regions and the stable higher branch. More specifically, when the excitation amplitude is large enough (e.g., f=0.014), the stability analysis between the semi-analytical and numerical methods is unsatisfactory.

The reduced model is expected to generate complex dynamic behaviors because it still has three strong nonlinearities. However, when only the frequency responses of the reduced model are compared with those of a system consisting of one linear oscillator and one cubic oscillator [32, 33], multiple unstable branches arise around the resonance frequency and two unstable branches are extended to the frequency band beyond the resonance frequency for a large excitation amplitude. Figure 5 shows the frequency responses of the cubic oscillators for f=0.006. Similar to the linear oscillator, it is observed that unstable branches of the first cubic oscillator are connected. However, unstable branches of the second and third oscillators are detached. In the present study, the semi-analytical method is used to find the branches of the studied system and further to guide the investigations on the differences in the energy transfer between these branches.

Figure 6 shows the system displacements for \Omega {\text{=}}1 and f=0.006. It is found that the system always has chaotic dynamics and its maximal response amplitude only changes slightly independent of the initial conditions. Accordingly, only a waveform with zero initial conditions is presented. Although the system has three unstable semi-analytical solutions whose values are quite different for this excitation, there is no significant difference between the responses with different initial conditions obtained by

Runge-Kutta method. Figure 7 reveals that the responses of the system with \Omega {\text{=0}} {\text{.98}} are periodic. The vibrations are unstable at the beginning of the response (also called the transient response) and energy transfers to small scales. However, the vibrations become stable rapidly and energy mainly localizes in the linear oscillator.

To further prove the chaotic state of the system, Lyapunov exponents are obtained where the responses in the last 1000 of 3000 (non-dimensional time) are used. The system (2) is transferred into state-space form involving eight variables, where four variables are related to the displacement and the other four variables reflect the velocity. Consequently, eight Lyapunov exponents are obtained. The results reveal that when \Omega {\text{=}}1, five Lyapunov exponents are positive while all Lyapunov exponents are negative for \Omega {\text{=0}}{\text{.98}}. Figure 9 illustrates the distribution of the average energy and the normalized energy flux which can be applied to evaluate the energy transfer between the oscillators. The input energy flux ({E_i}_{n}) and normalized energy flux ({\hat {E}_n}) between neighboring oscillators can be expressed as follows:

{E_i}_{n}=\int_{{{t_0}}}^{{{t_0}+T}} {f\cos (\Omega t)\,{{\dot {x}}_1}\,dt}
12a
{\hat {E}_n}=\frac{1}{{{E_i}_{n}{\varepsilon _n}}}{\text{ }}\int_{{{t_0}}}^{{{t_0}+T}} {{k_n}{{({x_n} - {x_{n+1}})}^3}{{\dot {x}}_{n+1}}\,dt}, n=1,\;2,...,N (12b)

Figure 9(a) shows that as chaotic responses occur, energy distributes in the entire chain, while it is concentrated on the linear oscillator when periodic responses generate. It is found that the average energy of the smaller oscillator is lower than that of the larger oscillator even if the chain produces chaotic responses. This phenomenon is attributed to the hierarchy of scales (i.e., the smaller oscillator has smaller mass and stiffness). However, the black straight line with a positive slope in Fig. 9(b) demonstrates that the energy transfer between the smaller oscillators is more intense than that between larger oscillators in a chaotic state. As expected, the energy transfer between smaller oscillators is weak in a periodic state.

Figure 10 shows the frequency responses of the cubic oscillators for f = 0.014. It is observed that the maximal unstable solution in the resonance band is close to solutions of the stable higher branch, which is quite different from the frequency response of the linear oscillator in Figure 4(b). Figures 11-13 show three typical responses. The responses in Figure 11 are obtained in the resonance band. The responses in Figure 12 and 13 are obtained for the same excitation frequency which is out of the resonance band, and different initial conditions. Considering the Lyapunov exponents in Figure 14, it is concluded that the three responses are chaotic. The responses obtained from the Runge-Kutta method in the chain with random initial conditions are chaotic, while the semi-analytical solutions for this excitation frequency are stable. It is noted that the results of stability analysis are consistent obtained by numerical and semi-analytical methods for relatively small excitation amplitudes. However, there exists some deviations between them for large excitation amplitudes. Even so, the semi-analytical results still can be used to assist the search

of the higher branches in the numerical study. Interestingly, the two significantly different responses obtained by Runge-Kutta method under the same excitation frequency are both chaotic.

In this section, the characteristics of the cross-scale energy transfer in the higher branch are compared with those in the lower branch. Figure 15(a) reveals that the energy distributions in the chain for \Omega {\text{=}}1 and \Omega {\text{=0}}{\text{.95}} with zero initial conditions are slightly different and the distribution rates in the four oscillators are consistent (black and red lines has the similar shape). Moreover, it is observed that the average energy in the chain for the higher branch of \Omega {\text{=0}} {\text{.95}} is much larger than those in the other cases. The same result can be achieved from the waveforms. Furthermore, the energy fluxes in the two cases with zero initial conditions are almost identical, while the energy flux in the case with non-zero initial condition is much lower than that in the former two cases, shown in Fig. 15(b). Accordingly, it is concluded that high levels of energy do not necessarily lead to a high energy transfer.

Then it is necessary to investigate the influence of the excitation amplitude on the cross-scale energy transfer of the oscillator chain with chaotic responses. In this regard, the results of two case studies are shown in Figs. 16 and 17. It is observed that as the excitation increases, the distributed energy in the three cubic oscillators monotonically increases in the resonance band (e.g., \Omega =1) except a special case (e.g., f=0.016). Moreover, the energy level of four oscillators increases slightly as the system generates a higher branch. This phenomenon may be attributed to difficulties in increasing the amplitude for a higher branch. The initial conditions for obtaining high branches in Fig. 17 are listed in Table 1. It is worth noting that the normalized energy fluxes almost remain constant in the two cases, indicating that the variations of the energy transfer between oscillators have a linear correlation with the increase of the input energy.

Table 1
Initial conditions for obtaining high branches in Fig. 17

	Initial conditions							
0.014	0.569	-0.522	-0.765	-0.211	-0.105	0.489	-0.091	-0.255
0.016	-0.693	-0.636	-0.203	-0.147	0.181	-0.533	-0.106	0.762
0.018	0.513	-0.268	0.118	-0.321	-0.038	0.311	-0.785	0.182
0.02	0.099	-0.165	0.492	0.209	0.283	-0.582	-0.308	0.423

Figures 18 and 19 show the influences of the scale (mass ratio) between cubic oscillators on the cross-scale energy transfer and the initial conditions are listed in Table 2. The oscillator chains produce chaotic responses. It is found that the energy level distributed in the cubic oscillators decreases with the increase of the mass ratio in both excitation conditions. Moreover, the distribution of normalized energy fluxes have the same slope and almost overlap with each other in Figs. 18(b) and 19(b). Recalling Fig. 15(b), the normalized energy flux of the oscillator chain has a significant difference as it produces two different vibration states. The responses in the lower and higher branches are deemed as two vibration states.

However, as the chain vibrates in one state, the normalized energy flux is almost independent of the variations of the input energy and the scale between cubic oscillators.

Table 2
Initial conditions for obtaining high branches in Fig. 19

Mass ratio	Initial conditions							
7	0.705	-0.177	0.024	-0.356	0.208	-0.591	0.164	0.209
8	0.569	-0.522	-0.765	-0.211	-0.105	0.489	-0.091	-0.255
9	0.062	0.381	0.527	-0.441	0.334	0.355	0.461	-0.261
10	-0.436	0.423	0.572	-0.102	0.263	-0.065	-0.028	0.089

4. Conclusions

In the present study, the cross-scale nonlinear energy transfer of a harmonically excited chain with a linear oscillator and three purely cubic oscillators as the chaotic responses occur is investigated. The performed analyses reveal that the chaotic dynamics of the three cubic oscillators are dominated by the strongly nonlinear stiffness in the oscillator chain. Accordingly, the complexification-averaging method and the least-square method are used to analyze the branches of response in the studied frequency band and to assist the search of the higher branches in the numerical study. The time histories of displacement and Lyapunov exponents of the system are used to determine the occurrence of chaotic responses. Moreover, the average energy and normalized energy flux are defined to evaluate the energy transfer in the oscillator chain.

The obtained results from the semi-analytical method are in good agreement with numerical results in terms of amplitude, but there are some deviations in lower- and higher-branches in terms of stability. The semi-analytical results show that the two additional small-scale cubic oscillators lead to complex branches of response around the resonance frequency of the linear oscillator in the lower branch. Moreover, the numerical results show that the oscillator chain can generate steady-state chaotic responses with entirely different amplitudes under the same excitation frequency.

Based on the obtained average energy and normalized energy flux of the oscillator chain with chaotic dynamics, it is concluded that the energy transfer patterns are similar in the same branch of response but quite different in different branches. It is noted that the dynamics in the higher branch are along with a lower energy transfer than that in the lower branch. Meanwhile, the normalized energy flux is almost independent of the variations of the input energy and the scale between cubic oscillators.

Declarations

Acknowledgement

This research was supported by the National Natural Science Foundation of China (Nos. 12172246, 11832002 and 11872274).

Conflict of interest

The authors declare that they have no conflict of interest.

Data Availability

All data included in this study are available from the corresponding author on reasonable request..

References

1. Balaji, P.S., Selvakumar, K.K.: Applications of nonlinearity in passive vibration control: a review. J. Vib. Eng. Technol. **9**, 183–213 (2020)
2. Jing, X.J., Vakakis, A.F.: Exploring nonlinear benefits in engineering. Mech. Syst. Signal Process. **125**, 1–3 (2019)
3. Ding, H., Chen, L.Q.: Designs, analysis, and applications of nonlinear energy sinks. Nonlinear Dyn. **100**(4), 3061–3107 (2020)
4. Lu, Z., Wang, Z.X., Zhou, Y., Lu, X.L.: Nonlinear dissipative devices in structural vibration control: a review. J. Sound Vib. **423**, 18–49 (2018)
5. Bak, B.D., Kalmar-Nagy, T.: A linear model of turbulence: reproducing the Kolmogorov-spectrum. IFAC PapersOnLine **51**(2), 595–600 (2018)
6. Kalmar-Nagy, T.: B. D. Bak. An intriguing analogy of Kolmogorov's scaling law in a hierarchical mass-spring-damper model. Nonlinear Dyn. **95**(4), 3193–3203 (2019)
7. Bak, B.D., Kalmar-Nagy, T.: Energy cascade in a nonlinear mechanistic model of turbulence. Technische Mechanik **39**(1), 64–71 (2019)
8. Chen, J.E., Theurich, T., Krack, M., Sapsis, T., Bergman, L.A., Vakakis, A.F.: Intense cross-scale energy cascades resembling "mechanical turbulence" in harmonically driven strongly nonlinear hierarchical chains of oscillators. Acta Mech., 2022, DOI:10.1007/s00707-022-03159-w
9. Vakakis, A.F.: Passive nonlinear targeted energy transfer. Philosophical Trans. Royal Soc. - Math. Phys. Eng. Sci. **376**(2127), 20170132 (2018)
10. Vakakis, A.F., Gendelman, O.V., Kerschen, G., Bergman, L.A., McFarland, D.M.: Y. S. Lee. Nonlinear targeted energy transfer in mechanical and structural systems, I and II. Springer, Berlin (2008)
11. O. V. Gendelman. Targeted energy transfer in systems with external and self-excitation. Proceedings of the Institution of Mechanical Engineers Part C: Journal of Mechanical Engineering Science, 2011, 225(C9): 2007–2043
12. Gendelman, O.V.: Transition of energy to a nonlinear localized mode in a highly asymmetric system of two oscillators. Nonlinear Dyn. **25**(1–3), 237–253 (2001)

13. Zang, J., Yuan, T.C., Lu, Z.Q., Zhang, Y.W., Ding, H.: L. Q. Chen. A lever-type nonlinear energy sink. J. Sound Vib. **437**, 119–134 (2018)
14. Geng, X.F., Ding, H., Mao, X.Y., Chen, L.Q.: Nonlinear energy sink with limited vibration amplitude. Mech. Syst. Signal Process. **156**, 107625 (2021)
15. GENG, X.F.: H. DING. Theoretical and experimental study of an enhanced nonlinear energy sink. Nonlinear Dyn. **104**(4), 3269–3291 (2021)
16. Geng, X.F., Ding, H.: Two-modal resonance control with an encapsulated nonlinear energy sink. J. Sound Vib. **520**, 116667 (2022)
17. Wei, Y.M., Wei, S., Zhang, Q.L., Dong, X.J., Peng, Z.K.: W. M. Zhang. Targeted energy transfer of a parallel nonlinear energy sink. Appl. Math. Mechanics-English Ed. **40**(5), 621–630 (2019)
18. Zhang, Z., Lu, Z.Q., Ding, H.: L. Q. Chen. An inertial nonlinear energy sink. J. Sound Vib. **450**, 199–213 (2019)
19. Chen, J.E., Sun, M., Hu, W.H., Zhang, J.H.: Z. C. Wei. Performance of non-smooth nonlinear energy sink with descending stiffness. Nonlinear Dyn. **100**(1), 255–267 (2020)
20. Zang, J., Cao, R.Q., Zhang, Y.W., Fang, B., Chen, L.Q.: A lever-enhanced nonlinear energy sink absorber harvesting vibratory energy via giant magnetostrictive piezoelectricity. Commun. Nonlinear Sci. Numer. Simul. **95**, 105620 (2021)
21. Xu, K.F., Zhang, Y.W., Zang, J., Niu, M.Q.: L. Q. Chen. Integration of vibration control and energy harvesting for whole-spacecraft: experiments and theory. Mech. Syst. Signal Process. **161**, 107956 (2021)
22. Moore, K.J., Bunyan, J., Tawfick, S., Gendelman, O.V., Li, S.B., Leamy, M.: A. F. Vakakis. Nonreciprocity in the dynamics of coupled oscillators with nonlinearity, asymmetry, and scale hierarchy. Phys. Rev. E **97**(1), 012219 (2018)
23. Mojahed, A., Gendelman, O.V., Vakakis, A.F.: Breather arrest, localization, and acoustic non-reciprocity in dissipative nonlinear lattices. J. Acoust. Soc. Am. **146**(1), 826–842 (2019)
24. Bunyan, J., Moore, K.J., Mojahed, A., Fronk, M.D., Leamy, M., Tawfick, S.: A. F. Vakakis. Acoustic nonreciprocity in a lattice incorporating nonlinearity, asymmetry, and internal scale hierarchy: experimental study. Phys. Rev. E **97**(5), 052211 (2018)
25. Wang, C.A., Tawfick, S., Vakakis, A.F.: Irreversible energy transfer, localization and non-reciprocity in weakly coupled, nonlinear lattices with asymmetry. Phys. D **402**, 132229 (2020)
26. Tsakirtzis, S., Panagopoulos, P.N., Kerschen, G., Gendelman, O., Vakakis, A.F.: L. A. Bergman. Complex dynamics and targeted energy transfer in linear oscillators coupled to multi-degree-of-freedom essentially nonlinear attachments. Nonlinear Dyn. **48**(3), 285–318 (2007)
27. Grinberg, I., Lanton, V.: O. V. Gendelman. Response regimes in linear oscillator with 2DOF nonlinear energy sink under periodic forcing. Nonlinear Dyn. **69**(4), 1889–1902 (2012)
28. Taghipour, J., Dardel, M.: Steady state dynamics and robustness of a harmonically excited essentially nonlinear oscillator coupled with a two-DOF nonlinear energy sink, Mechanical Systems

and Signal Processing, 2015, 62–63: 164–182

29. Charlemagne, S., Lamarque, C.H., Savadkoohi, A.T.: Vibratory control of a linear system by addition of a chain of nonlinear oscillators. Acta Mech. **228**(9), 3111–3133 (2017)
30. Lee, Y.S., Vakakis, A.F., Bergman, L.A., McFarland, D.M.: G. Kerschen. Enhancing the robustness of aeroelastic instability suppression using multi-degree-of-freedom nonlinear energy sinks. AIAA J. **46**(6), 1371–1394 (2008)
31. Wierschem, N.E., Luo, J., AL-Shudeifat, M., Hubbard, S., Ott, R., Fahnestock, L.A., Quinn, D.D., McFarland, D.M., Spencer, B.F., Vakakis, A.F.: L. A. Bergman. Experimental testing and numerical simulation of a six-story structure incorporating two-degree-of-freedom nonlinear energy sink. J. Struct. Eng. **140**(6), 04014027 (2014)
32. Sun, M., Chen, J.E.: Dynamics of nonlinear primary oscillator with nonlinear energy sink under harmonic excitation: effects of nonlinear stiffness. Mathematical Problems in Engineering, 2018, 2018: 5693618
33. Starosvetsky, Y., Gendelman, O.V.: Vibration absorption in systems with a nonlinear energy sink: nonlinear damping. J. Sound Vib. **324**, 916–939 (2009)

Figures

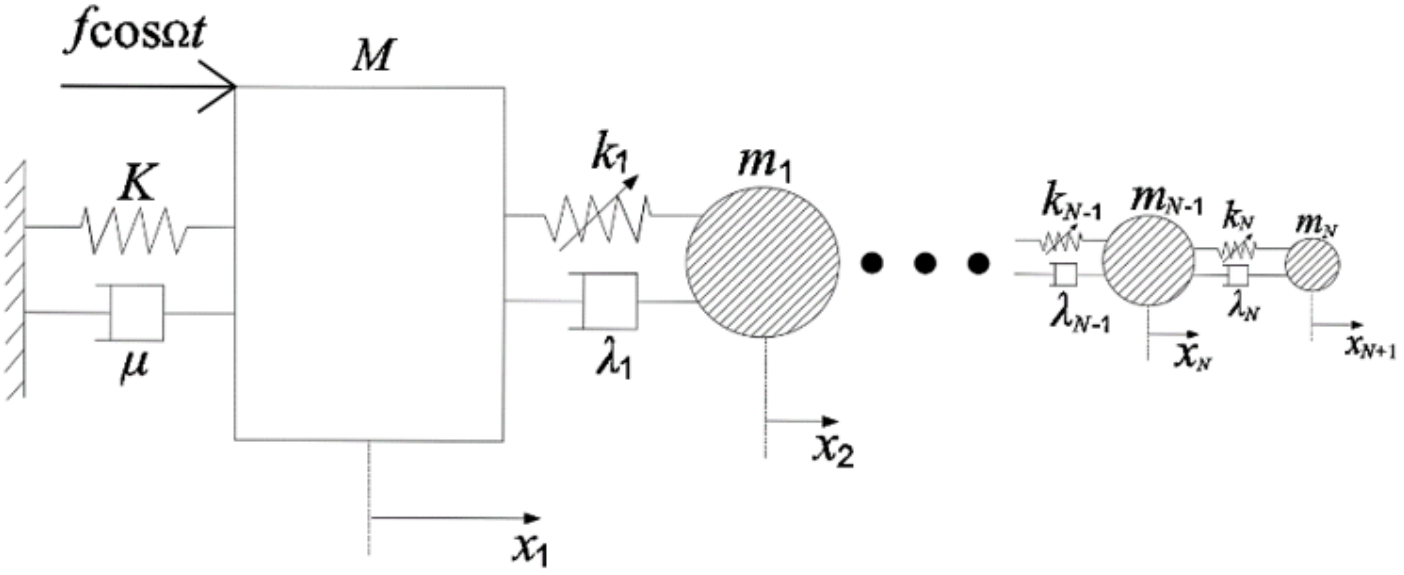

Figure 1

Mechanical model of a cross-scale oscillator chain

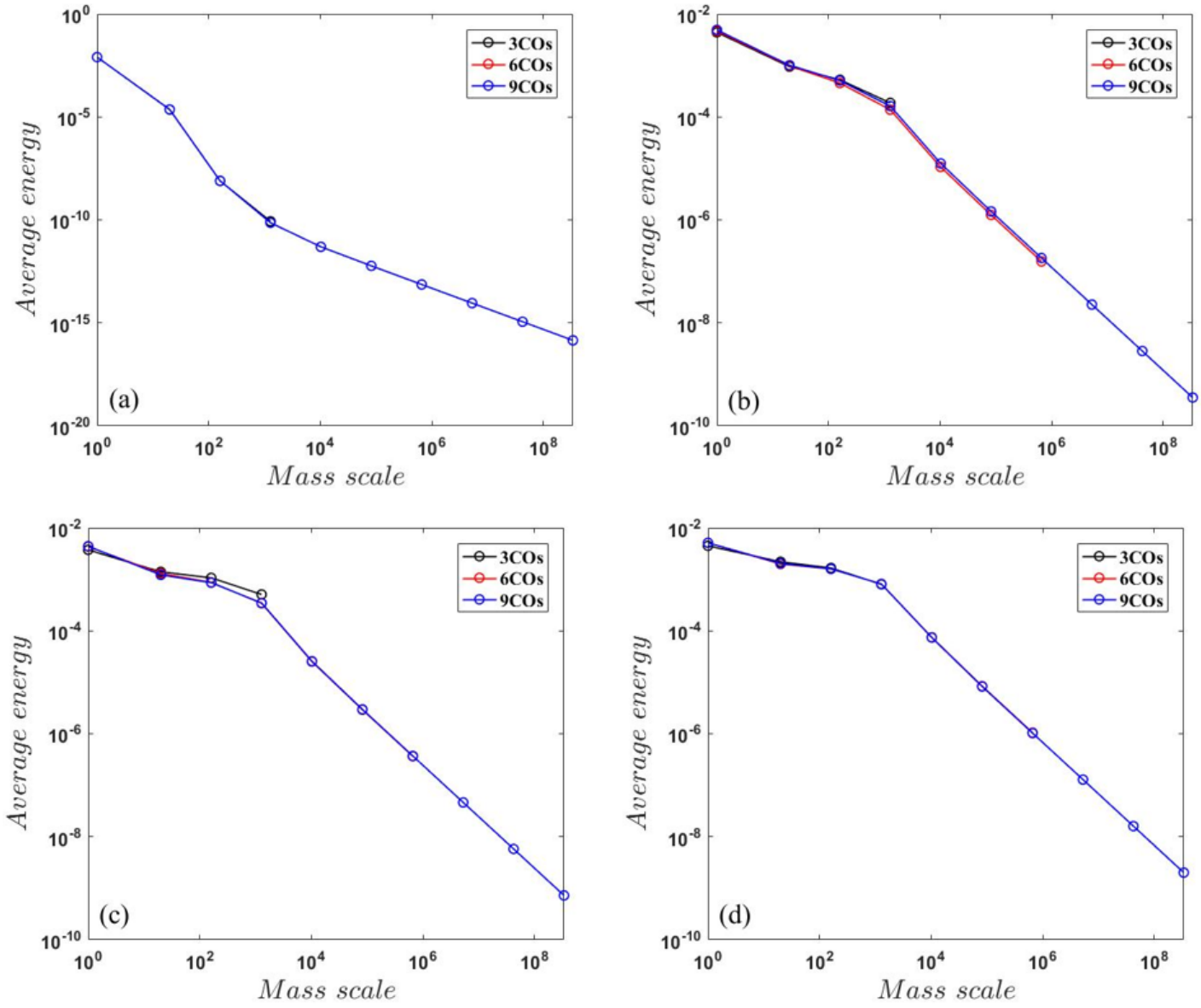

Figure 2

Distribution of average energy of the chain with different numbers of oscillators, Ω=1 and (a) f = 0.002 , (b) f = 0.006 , (c) f = 0.001 , and (d) f = 0.014.

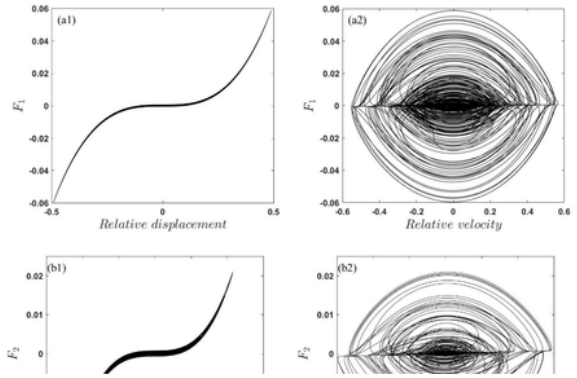

Figure 3

Dominate ranges of the chain with six oscillators for Ω=1 and f=0.006.

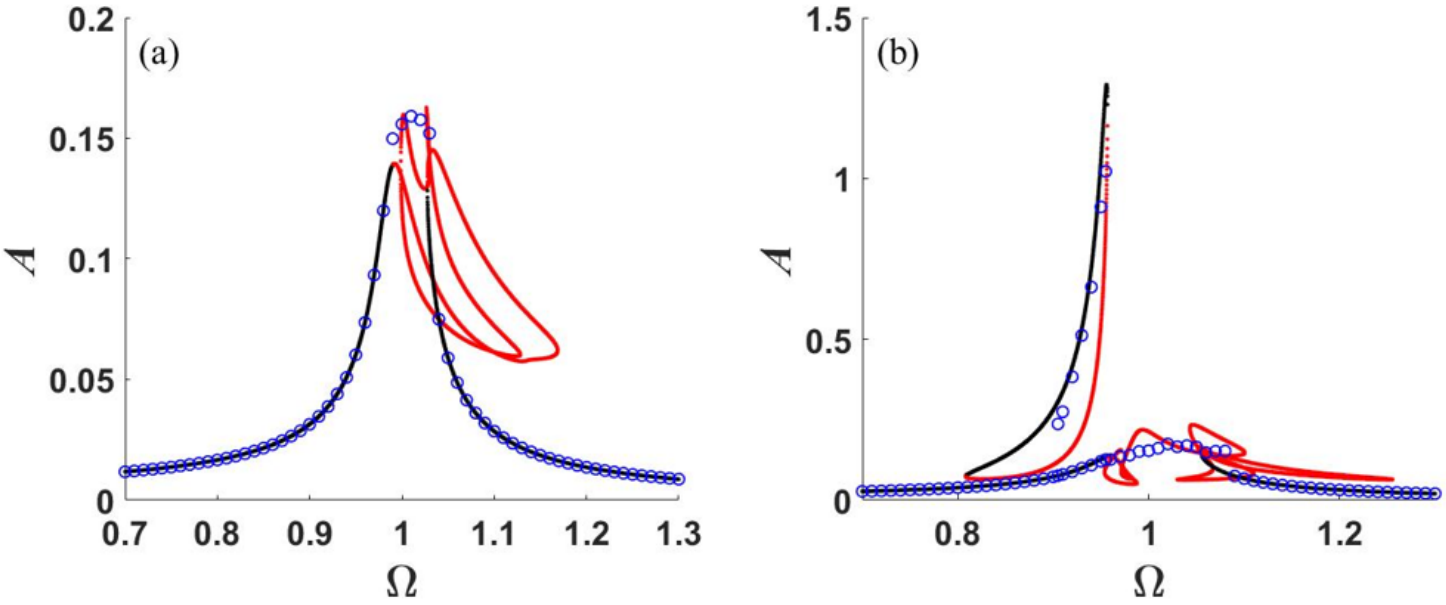

Figure 4

Verification of the derivation (Frequency responses of the linear oscillator) (a) f = 0.006, (b) f = 0.014.

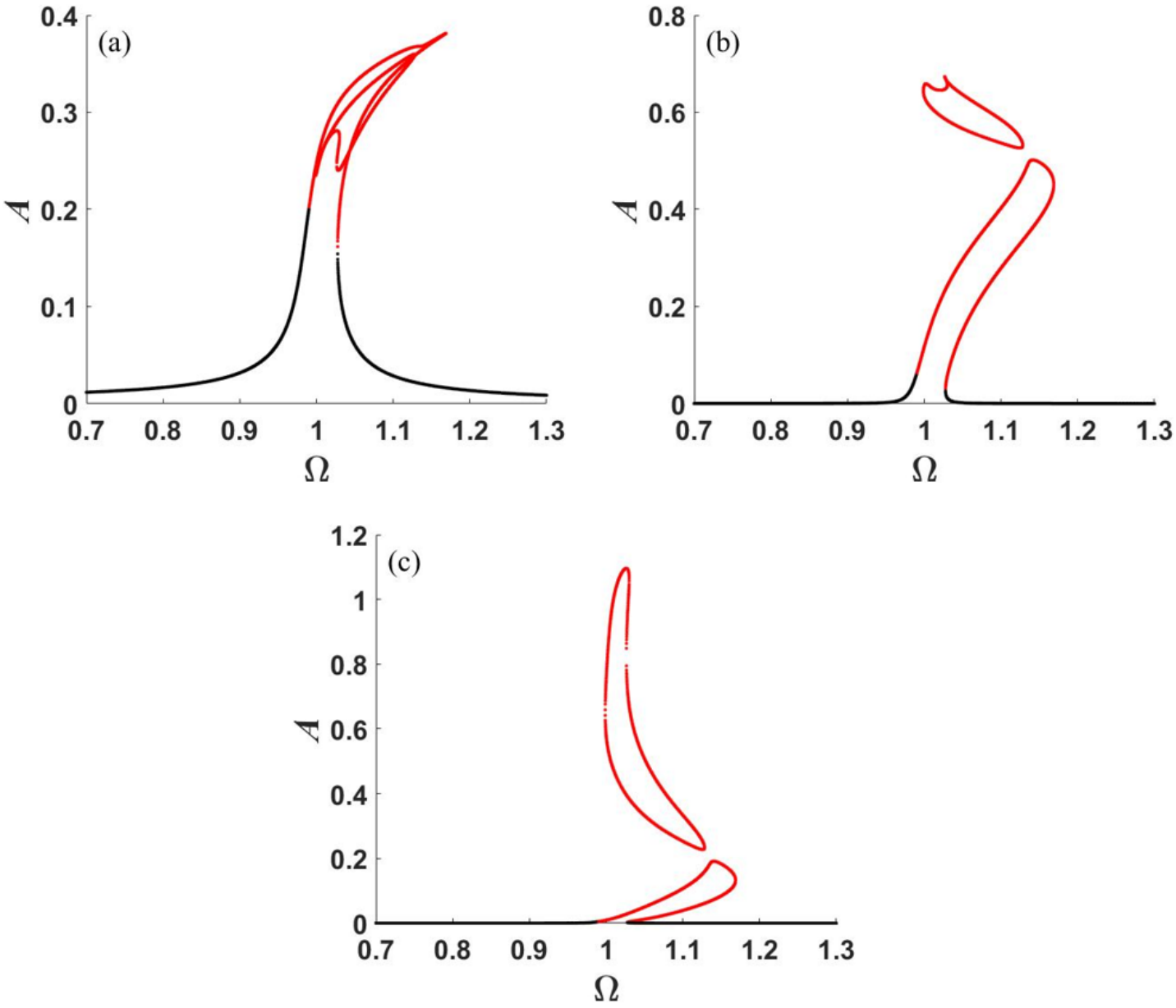

Figure 5

Frequency responses of (a) the first cubic oscillator, (b) the second cubic oscillator, and (c) the third cubic oscillator for f=0.006.

Figure 6

Displacements of (a) the linear oscillator, (b) the first cubic oscillator, (c) the second cubic oscillator, (d) the third cubic oscillator for Ω=1 and f = 0.006 with zero initial conditions.

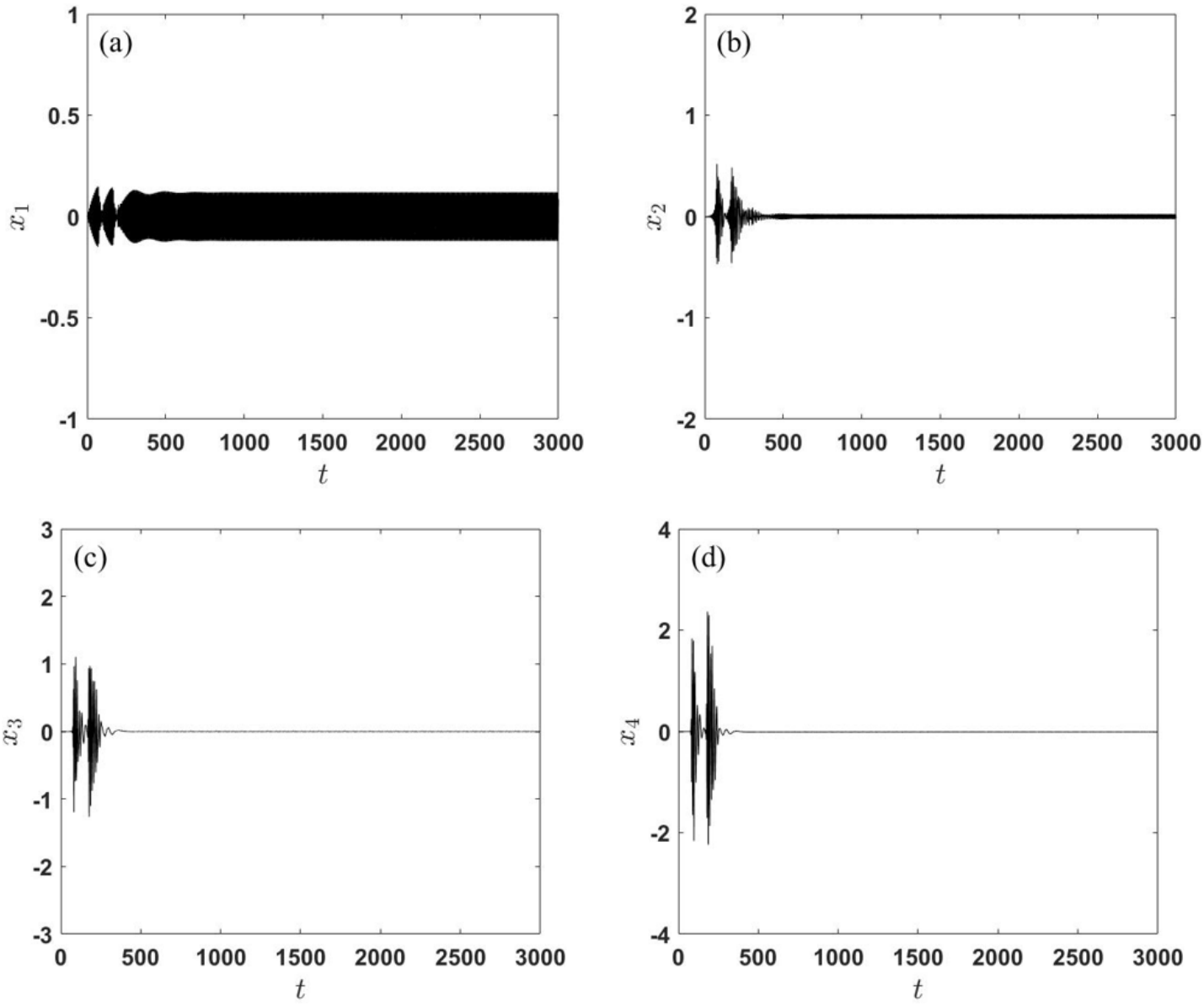

Figure 7

Displacements of (a) the linear oscillator, (b) the first cubic oscillator, (c) the second cubic oscillator, and (d) the third cubic oscillator for Ω = 0.98 and f = 0.006 with zero initial conditions.

Figure 8

Lyapunov exponents of the four oscillators for f = 0.006 and (a) Ω=1 and (b) Ω=0.98 .

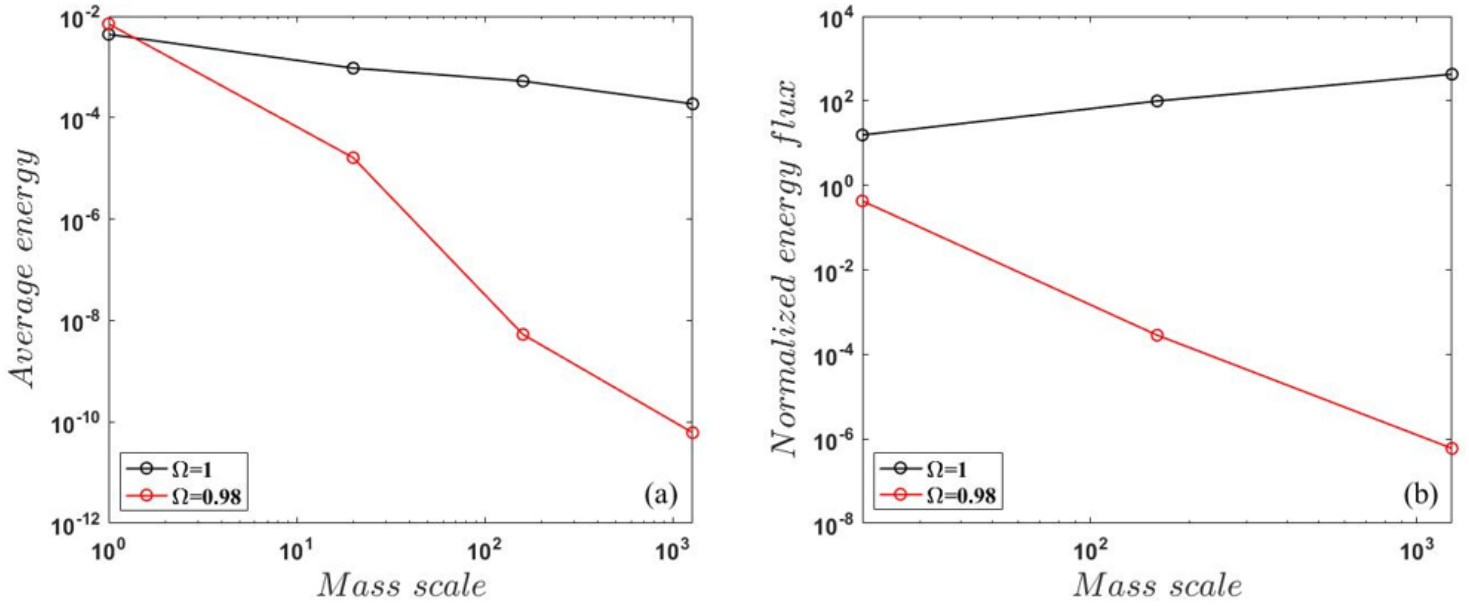

Figure 9

Irreversible large-to-small scale nonlinear energy cascading and energy transfer for f = 0.006 , (a) average energies; (b) normalized energy fluxes.

Figure 10

Frequency responses of (a) the first cubic oscillator; (b) the second cubic oscillator; (c) the third cubic oscillator for f = 0.014.

Figure 11

Displacements of (a) the linear oscillator, (b) the first cubic oscillator, (c) the second cubic oscillator, (d) the third cubic oscillator with Ω=1, f = 0.014 and zero initial conditions.

Figure 12

Displacements of (a) the linear oscillator, (b) the first cubic oscillator, (c) the second cubic oscillator, (d) the third cubic oscillator with eΩ=0.95 , f = 0.014 and zero initial conditions.

Figure 13

Displacements of (a) the linear oscillator, (b) the first cubic oscillator, (c) the second cubic oscillator, (d) the third cubic oscillator with Ω=0.95, f = 0.014 and non-zero initial conditions (0.049, -0.635, 0.011, 0.301, 0.449, -0.049, -0.792, -0.257).

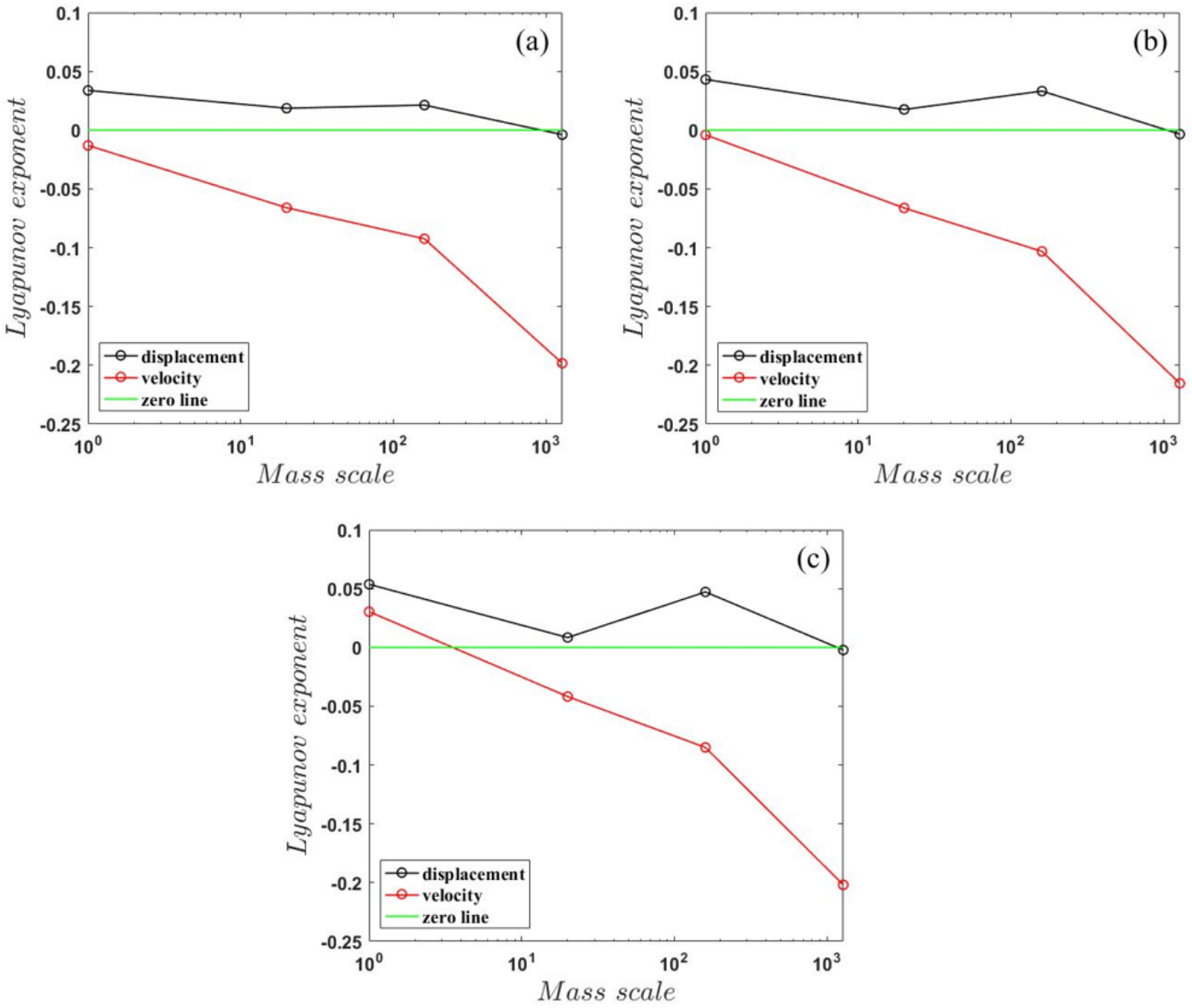

Figure 14

Lyapunov exponents of the four oscillators with f = 0.014 and (a) Ω=1 , (b) Ω=0.95 and zero initial conditions (c) Ω=0.95 and non-zero initial conditions.

Figure 15

Large-to-small scale nonlinear energy transfer with f = 0.014, (a) average energies, (b) normalized energy fluxes.

Figure 16

Large-to-small scale nonlinear energy transfer with $\Omega = 1$, zero initial conditions, and different forces. (a) average energies, (b) normalized energy fluxes.

Figure 17

Large-to-small scale nonlinear energy transfer with $\Omega = 0.95$, non-zero initial conditions and different forces. (a) average energies, (b) normalized energy fluxes.

Figure 18

Distributions of the (a) average energy and (b) normalized energy flux against the mass scale for different mass rations with $\Omega = 1$, $f = 0.014$ and zero initial conditions.

Figure 19

Distributions of the (a) average energy and (b) normalized energy flux against the mass scale for different mass rations with $\Omega = 0.95$, $f = 0.014$ and non-zero initial conditions.